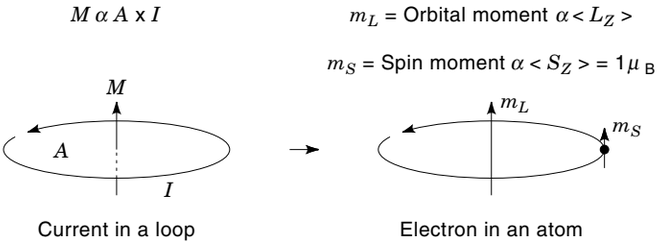

Figure 1. Source of the atomic magnetic moment. At left is the dipole moment generated by a current in a loop of wire. At right is the moment in an atom generated by the electron orbital motion and spin.

MAGNETIC STRUCTURE

The identification and characterization of the magnetic structure of a material depends on the viewpoint from which the characterization is required. At a strictly atomistic level, the relevant magnetic structure may be the relative orientation of the magnetic moment of one atom with respect to other atomic moments (these other moments may be made of the same or different elements), or it may be the relative orientation of the atomic magnetic moment with respect to the crystalline axes of the material. At the nanoscopic or microscopic level the magnetic structure may refer to the relative ordering of magnetic domains, magnetic particulates, or small magnetic structures which have formed within the material. For an artificially structured multilayer film, it may constitute the orientation of the magnetic directions of each film in the layered system, or it may refer to the correlation of magnetic domains between layers. In each case, from each of these distinct viewpoints, a knowledge of the magnetic structure of the film, and its evolution with external influences (like an applied magnetic field) would be very beneficial in understanding the overall behavior of the system.

SOURCE OF MAGNETISM

In an introduction to magnetic structure it is always useful to briefly outline the underlying source of the atomic magnetic moment. There are two contributions to the total magnetic moment of an atom, the spin-moment, m_S, and the orbital-moment, m_L. An intuitive view of the source of the atomic magnetic moment can be obtained by analogy with the magnetic properties of a loop of wire carrying a current, as described in Fig. 1. As in an electromagnet, the current carried in a loop of wire creates a magnetic field which, at distances from the loop much larger than the loop diameter, can be adequately modeled by a magnetic dipole positioned at the center of the loop pointing upward (z-direction) according to the right-hand rule. In this mathematical simplification the moment generated by the current flowing in the loop is proportional to the product of the current in the loop, I, and the area enclosed by the loop, A. These two parameters characterize the strength of the magnetic dipole, and therefore the magnetization felt at a distance from the loop.

A simplistic view of an electron in an atom portrays the electron (charge) moving in an orbit around the nucleus. (A rigorous treatment can be found in Ref. 1.) This moving charge can be viewed as generating a magnetic field similar to the moving charge in a loop of wire, but in this case the area of the loop must be treated in quantum mechanical terms. The resulting magnetic dipole caused by the orbital motion of the electron, termed the orbital-moment, m_L, is proportional to the electron charge multiplied by the expectation value of the angular momentum of the electron (L) projected along the z-axis (z-component of L, labeled L_Z). But, unlike the current in a loop, the electron in an atom has a second contribution to the total magnetic moment. In addition to the intuitive orbital-moment, the individual electrons possess an intrinsic spin-moment which is proportional to the expectation value of the quantum mechanical spin of the electron (S), projected along the z-axis (S_Z component) which can only have a value of $+\frac{1}{2}$ or $-\frac{1}{2}$. The moment of a single electron spin is equal to 1 bohr magneton (1 μ_B). For a multielectron atom the total magnetic moment of the atom is the sum of the various orbital and spin-moment contributions of each electron of the atom.

The atomic moment forms the basic building block of magnetic structure in condensed materials. Interactions between the atomic moments, constrained by the imposed crystallographic architecture, form macroscopic spin structures. This article will not discuss the atomistic magnetic structures generated from these interactions between the individual magnetic moments. [The magnetic ordering can be incompletely classified in the standard way: diamagnetism, paramagnetism, antiferromagnetism, ferromagnetism, metamagnetism, superparamagnetism, ferrimagnetism, and parasitic ferromagnetism; (see Refs. 2 and 3)]. Instead, because of the tremendous advancements in thin film magnetism for application as magnetic devices, this report will focus on characterizing the nanoscale and microscale magnetic struc-

tures, especially those generated in thin film and multilayer magnetic structures.

DETERMINING MAGNETIC STRUCTURE

The complex and intricate interplay among material properties, thin film morphology, lithographic processing, and micromagnetic dynamics of the new classes of magnetic materials and devices lead us to anticipate a variety of barriers to their successful implementation as magnetic memories and magnetic based sensors (4,5). Since these devices are multilayered, multielement, and heteromagnetic (more than one magnetically active element) and because the vast majority of magnetic techniques cannot separate the magnetic signatures of the various materials, it is clear that an element-specific, layer-sensitive magnetic order probe to determine the magnetic structure is needed.

Most standard magnetic characterization tools are not sensitive to the atomic type but instead give the total magnetic moment of the sample within the probed volume. The few exceptions are usually only sensitive to one atomic species and are not broadly useful. A new direction in magnetic characterization that does have broad-based element selectivity exploits recent advancements in the use of synchrotron radiation facilities (6). These large experimental facilities serve as sources for the generation of intense X rays and are a powerful and proven tool for basic and applied studies in biology, chemistry, material science, medicine, and physics and their related subfields (6).

Magnetic Circular Dichroism

Whenever a charged particle undergoes an acceleration, it emits electromagnetic radiation. If high-energy electrons traveling at relativistic speeds (near the speed of light) are constrained to move in a circular orbit by the strong magnetic fields of a vacuum storage ring, the resulting emitted radiation, termed synchrotron radiation, is extremely intense and varies over a very broad range of wavelengths from infrared through visible and into soft and hard X rays. It turns out that this intense, highly collimated emitted radiation is also strongly polarized. Due to the dipole character of the synchrotron radiation, X rays emitted in the plane of the synchrotron (the plane-of-orbit of the circulating electrons) are linear polarized (6). Collecting X rays emitted out of the plane of the synchrotron (either above or below the plane-of-orbit) yields X rays with a high degree of left circular or right circular polarization (they are actually elliptical polarized X rays). Although many uses have been made of the linear polarized photons, it is the interaction of these left and right circular polarized X rays (also referred to as positive or negative helicity photons) with the spin-polarized electrons in magnetic materials that gives this technique element selectivity and magnetic sensitivity.

Magnetic circular dichroism (MCD) is a term used to describe a technique whose underlying mechanism is simply the difference between the absorption of left and right circular polarized photons by a magnetic material (7–13). MCD is complementary to the many, more familiar, spin-resolved electron techniques, but instead of resolving or selecting the electron spin, it uses the photon selection-rules associated with the absorption of circular polarized X rays to probe the wave-function character (spin + symmetry) of the unfilled electron states of the material. The MCD measurements are much more sensitive than electron spin-detection or spin-selection techniques [the figure-of-merit for MCD is 2 orders of magnitude higher than spin detection; see (8,14)] and can be acquired in the presence of magnetic fields. Also MCD measurements are element and even site specific with high sensitivity, enabling radically new experiments for unique insights into magnetic structures and interactions.

MCD is a technique that has element selectivity and magnetic sensitivity. The element specificity of MCD is generated from the same mechanism as that of X ray absorption spectroscopy. The electronic structure of a magnetic material (particularly the itinerant magnet materials of the transition metals) can be described in a picture where the available electron states are separated by their spin direction (up or down). In Fig. 2 is shown the number of available states for the electrons of a magnetic material as a function of the energy of the state, but separated by the electron spin. In this spin-resolved density-of-states picture, the right side represents the majority-spin (up-spin) states, and the left side the minority-spin (down-spin) states where the dotted line represents the fermi energy, E_f, separating the occupied and unoccupied states. (There are more up-spin electrons in the material, hence the term majority-spin electrons.) Shown at much deeper binding energies are the electrons of the spin-orbit split $2p_{3/2}$ core level (associated with the L_3 absorption edge) and the $2p_{1/2}$ core level (associated with the L_2 absorption edge).

For an incident photon, as the energy of the photon is increased, it reaches a value that is sufficient to promote a bound electron from the $2p_{3/2}$ core level up to the unfilled states above the fermi level, resulting in an increase in the photoabsorption by the sample. Since the binding energy of the $2p_{3/2}$ electron depends on the number of protons in the nucleus (and to a much lesser extent the chemical environment of the atom), the energy needed to promote the $2p_{3/2}$ electron, or the binding energy of the electron, will be different for different elements. Using photon energies near a particular absorption edge of an element will only probe the elec-

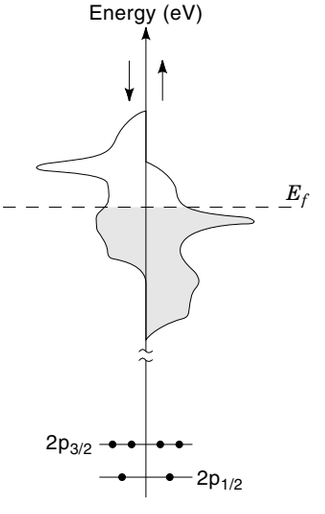

Figure 2. Electronic states available in a magnetic material separated by the electron spin direction. The fermi level, E_f, separates the occupied and unoccupied states.

tronic structure of that element, making this technique chemical specific.

The magnetic selectivity rises from the fact that for a circular polarized photon, the probability that the photon is absorbed by a magnetic material depends on the relative orientation of the spin of the electron and the spin of the photon. [The photon spin is defined by whether the photon rotation, or spin, is to the right (up spin) or the spin is to the left (down spin).] There is a large difference in the absorption of a magnetic sample depending on whether these two spin directions are aligned or anti-aligned. This is clearly demonstrated in Fig. 3 where is shown the X-ray absorption spectra of Fe for the two photon polarizations (helicities), corresponding to when the photon and electron spin directions are aligned and antialigned. The MCD (not shown) is just the difference of these two absorption spectra. Note that in Fig. 3, the L_3 and L_2 absorption edges have opposite MCD, characteristic of the transition metals.

EXAMPLES

To illustrate the utility of MCD in characterizing magnetic structures, three examples are described below to illustrate increasingly sophisticated characterization of the magnetic structure. Each of these measurements were conducted at the Naval Research Laboratory/National Synchrotron Light Source (NRL/NSLS) Magnetic Circular Dichroism Facility located at the NSLS Beamline U4B (15).

Elemental Selectivity: Cr/Fe(001)

The most straightforward application of MCD is to determine in which elements of a material are ferromagnetic and in which direction their moments point. This is extremely useful in examining alloy systems, overlayer systems, and buried layers. Therefore, in this first example, the presence of an MCD signal in the L-edge spectra of an element is used as a clear indication that the element is ferromagnetic and that it posses a net magnetic moment. What is more, the sign of the MCD is indicative of the moment direction, allowing for the determination of the relative moment orientations in samples with more than one magnetic element. Used first in the hard X-ray (14) and later in the soft X-ray regions (9), this straightforward and simple variant of MCD is now used at NSLS and by a variety of other groups to unambiguously identify the presence of ferromagnetism or induced moments in an element-specific and site-specific manner. MCD in absorption has been used to identify induced moment and relative moment orientations for transition metals and rare earths deposited on ferromagnetic substrates where the magnetic signature of the substrate would completely mask the very small response of the overlayer (10).

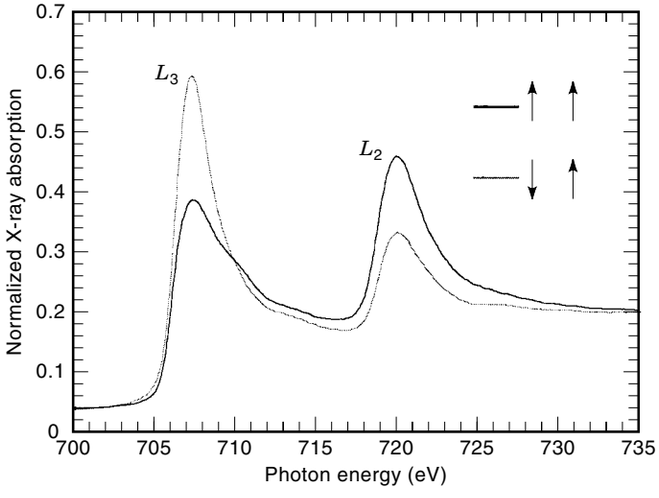

Figure 3. Typical transition metal magnetic circular dichroism (MCD) spectra. Solid line for aligned spins, dotted line for antialigned spins. Note that the L_3 and L_2 edges have opposite MCD behavior.

To exploit the unique capabilities of MCD, namely its element specificity, reported here are MCD measurements for the determination of the magnetic structure of one monolayer (ML) of Cr deposited on single crystal body-centered cubic (bcc) Fe(001) (10). This system is of interest because it is the preliminary stage for the development of the Fe/Cr/Fe heterostructure which is representative of a class of layered systems that display aligned or antialigned coupling of the two ferromagnetic films through the interlying spacer layer (16–19), where the sign of the coupling is dependent on the thickness of the spacer layer (20).

To generate and maintain a clean single monolayer Cr overlayer, the sample is created in an ultra-high vacuum growth chamber with a base pressure of 1×10^{-10} torr. First, the Fe is deposited from a vacuum furnace on a GaAs(001) substrate which has been heat-cleaned in vacuum at 580°C to generate an oxide-free GaAs(001) surface. The Fe is deposited with the substrate held at 175°C and at a vacuum of 2×10^{-10} torr until a 150 Å Fe body-centered cubic (bcc) film is developed (10). This film is single crystal and displays the magnetic properties associated with the bcc Fe magnetic structure (21). A subsequent growth of Cr is carried out with the sample held at room temperature to eliminate interdiffusion and alloying between the Cr and the Fe.

The top panel of Fig. 4 shows the two room temperature X-ray absorption spectra (XAS) and the difference spectra (MCD) of the L_3 and L_2 absorption edges of the as-deposited first Fe film as a function of the soft X-ray energy. The solid line is taken with the spin direction of the photons parallel to that of the majority electrons of the Fe film, while the dashed line is taken with antiparallel spin directions. The dots are the difference between the parallel and antiparallel spectra which is the magnetic circular dichroism (MCD). After the 150 Å thick Fe film is measured, we deposit a fractional (0.25 ML) Cr overlayer. Unlike the layer-by-layer growth of Cr on unstressed Fe whiskers at elevated temperatures (19,22), we have found that the room temperature deposition of Cr on thin Fe films deposited on heat-cleaned GaAs(001) substrates form three-dimensional islands. The differences may be due to the rough nature of the surface of the Fe/GaAs(001) (23). Because the Cr grows in 3-D islands on the Fe/GaAs(001), submonolayer coverage down to 0.25 ML were recorded to maximize the amount of Cr in the first layer position and minimize the presence of Cr in second layer sites.

The bottom panel of Fig. 4 show XAS and MCD spectra of the lowest coverage, 0.25 ML Cr film. Because the 2p electron binding energies differ for different materials, these absorption L edges occur at different photon energies (see Fig. 4), yielding the elemental selectivity. At 0.25 ML coverage nearly

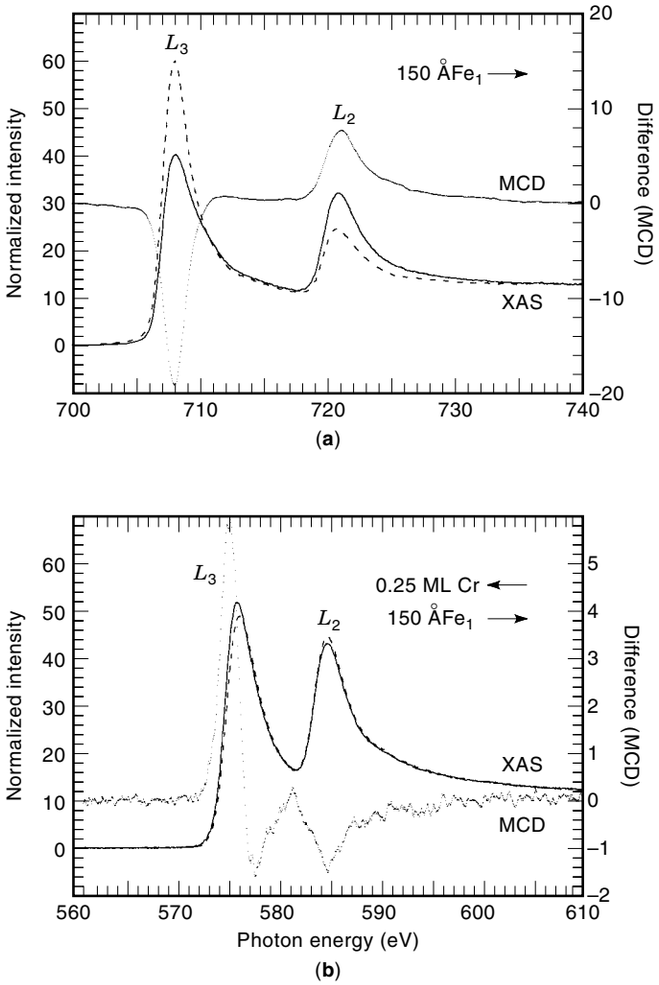

Figure 4. MCD spectra demonstrating that 0.25 ML of Cr has a magnetic moment aligned opposite to Fe moment. Top panel is absorption (XAS) and difference (MCD) scans for Fe; bottom panel is XAS and MCD for Cr with solid line for aligned spins, dashed for antialigned, and dots difference spectra.

all the deposited Cr should occupy the first layer with very little in second layer sites. Since MCD is element specific, it is immediately evident from the reversal of the Cr MCD intensity at both the L_3 and L_2 edges in comparison to the Fe MCD spectra, that submonolayer coverage of Cr are ferromagnetic and antialigned with the first Fe layer (as depicted in the inset of Fig. 4). If the Cr were not magnetic, no MCD signal would be detected. This alignment is in agreement with theoretical calculations for single monolayer Cr/Fe(001) structures which also predicted a ferromagnetic Cr layer adjoining to and antialigned with the Fe films (24–26). In addition to the reversal of the MCD signal, the Cr data show a strong differentiationlike lineshape at the L_3 edge which is due to a peak energy shift between the two XAS spectra, resembling the result of a recent atomic multiplet and crystal field calculation (27).

This example demonstrates that by simply inspecting the separate MCD signals of the overlayer and the magnetic substrate material, the relative orientation of the two moments created from the strong coupling of the moments at the interface can be determined. This effect has been used in a wide variety of overlayer systems to determine the relative magnetic structure of induced moments of materials in close proximity to a ferromagnetic substrate. Similarly this inspection method has been used in multielement alloys to determine the magnetic role that each element plays (28) and to identify absorbate Curie temperatures (29).

Element-Specific Magnetometry

In the previous discussion of MCD, it was pointed out that it is the relative orientations of the spin of the electron and the spin of the photon that mediate the absorption strength of the material. By changing the photon spin direction, we can generate the MCD spectra and determine the magnetic state of the element. But, instead of reversing the photon spin direction, it is equivalent to reverse the electron spin direction (through the reversal of the magnetization of the sample by applying a magnetic field). In fact simultaneously reversing both the photon and electron spin direction MUST result in the same absorption and MCD spectra, since it is only the relative orientation of the two that is important. The benefit to reversing the electron spin directions is that we can now measure the MCD intensity, which is proportional to the net magnetization of that element within the material, *as a function of magnetic field.* These spectra now reflect the variation of the elemental moment as a function of applied magnetic field, and they serve as an element-specific magnetometer.

If the MCD is measured in transmission or by fluorescence detection by reversing the applied magnetic field direction while keeping the polarization of the incident photon beam fixed, this method permits for the measurement of element-specific magnetic information in an applied field intensity. In particular, by monitoring the peak height of a given elemental absorption edge (typically the L_3 white line) as a function of the applied magnetic field, element-specific magnetic hysteresis curves can be obtained (30).

The utility of element-specific magnetometry was demonstrated at NSLS where the element-specific hysteresis curves were measured and compared to the total hysteresis curve for a multilayer sample consisting of a Co (51 Å)/Cu (30 Å)/Fe (102 Å) trilayer structure deposited on a glass substrate and capped with an additional Cu film (40 Å) to prevent oxidation (see Fig. 5). Multilayer films of this type have important applications in magnetic read-heads and as elements in ultradense, nonvolatile memory. The top panel of Fig. 5 shows the measured MCD intensity for the Fe L_3 and Co L_3 absorption edge as a function of the applied magnetic field. These are the element-specific magnetic hysteresis loops. The bottom panel shows the total moment hysteresis curve as measured by vibrating sample magnetometry (shown as a solid line labeled VSM). Superimposed on the VSM hysteresis curve of the bottom panel is the scaled sum of the two individual Fe and Co element-specific magnetic hysteresis curves (shown as a dashed line labeled Fe + Co). The agreement is nearly perfect. From these scaling values, the known Co and Fe film thicknesses, and the total magnetic moment value as measured by VSM, the average elemental atomic magnetic moment of the Fe and the Co can be extracted. Our best fit determines the average moments to be 2.1 μ_B for the Fe and 1.2 μ_B for the Co.

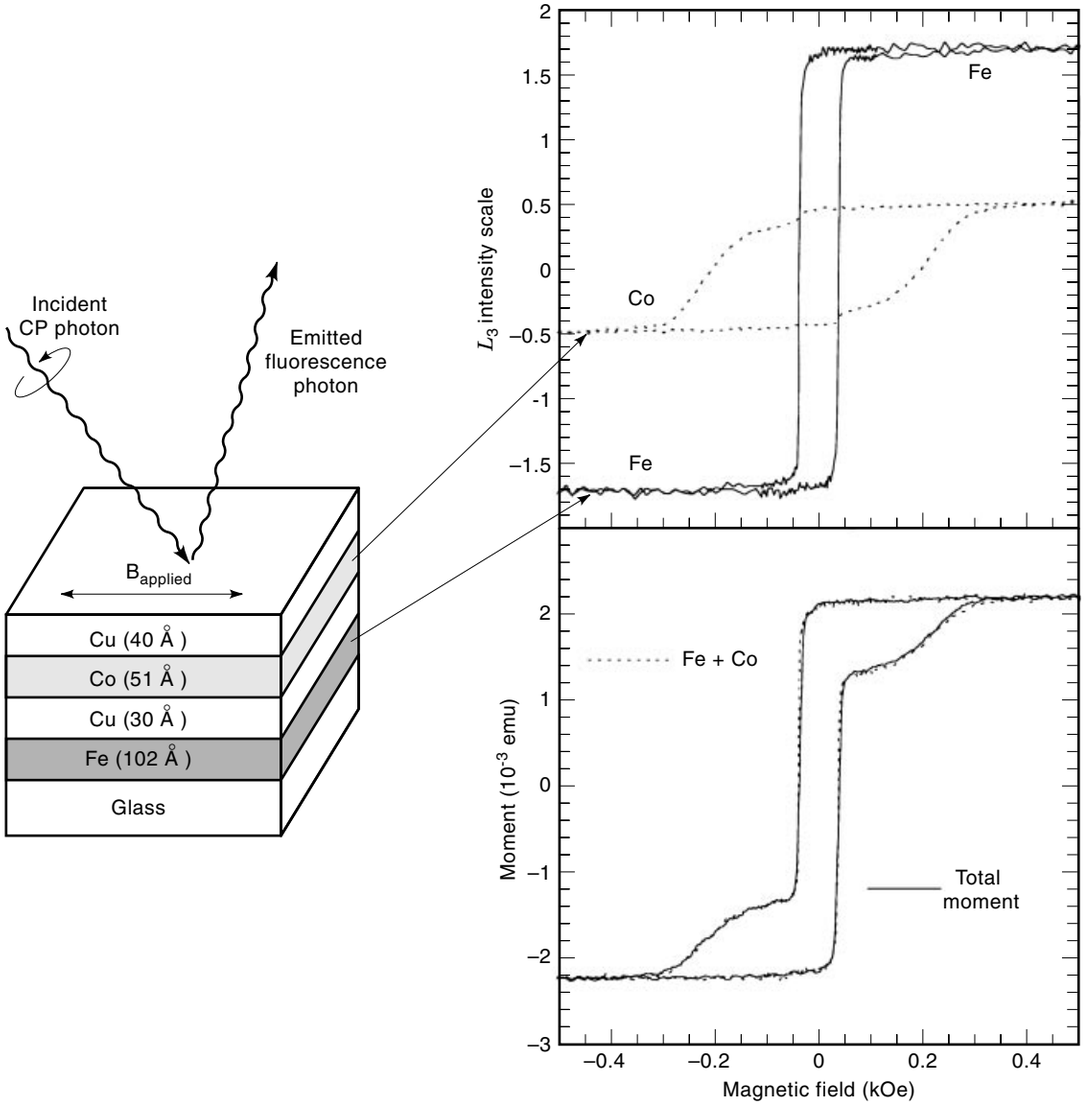

Figure 5. Element-specific hysteresis curve for Fe/Cu/Co multilayer. Left panel shows multilayer configuration. Top right panel shows L_3 intensity as a function of applied magnetic field for Fe and Co, these are the element-specific magnetic hysteresis curves. Bottom right panel shows total moment magnetometry curve (solid line) and sum of scaled Fe and Co curves (dotted line). The agreement is exact.

Figure 5 describes the dissection of a magnetometry curve into its chemically distinct parts for magnetic moment determination. Although this allows for the determination of individual moments or for the extraction of coefficients of magnetoresistance (31), this process was undertaken for only one component of the magnetic moment vector. By recording all three components of the magnetic moment vector sequentially, a coherent picture of the magnetic moment behavior as a function of applied field for each element is obtainable. This powerful technique of element-specific vector magnetometry (ESVM) is accomplished through the use of an in situ electromagnet which permits either independent or concerted rotation of the sample and the magnet with respect to the photon beam direction (32).

A powerful application of ESVM is for the characterization of buried magnetic layers. In a recent measurement of a Co/Mn/Co trilayer system (33), the rotation and reversal of the Mn and Co magnetic moment vectors were determined as a function of applied field. In this system the two ferromagnetic films are coupled at an angle through the interlying Mn film (34), this coupling angle is dependent on the thickness, and therefore the magnetic structure of the Mn film. From the element-specific vector magnetometry curves of Co and Mn, the magnetic structure of the Mn was determined to be an antiferromagnetic helix, resembling the recent theoretical predictions for frustrated moment systems (35). This is the only method that could identify the applied field dependent variation of the extremely small Mn moment. All other total moment techniques would only measure the comparatively very large signature of the enclosing ferromagnetic films where the minuscule signal associated with the Mn would be lost.

Identifying Layer Switching

So far we have been investigating only the differential absorption of circular polarized photons by a magnetic heterostructure. Complimentary to this technique is the study of the differential reflectivity of circular polarized photons from a magnetic multilayer. Variants of XRMS have been used to identify layer thicknesses with high accuracy, characterize layer switching (36), and determine interfacial parameters, including separately measuring the chemical and magnetic roughness of the interface (37).

As a technologically relevant example of the importance of magnetic structure characterization at these larger scales, Fig. 6 shows a cartoon of a lithographically patterned trilayer magnetic device which can be used as an element in the next generation of magnetic memory. The structure consists of a conducting substrate onto which has been deposited two ferromagnetic films separated by a nonmagnetic spacer layer and capped with a metallization layer. The multilayer film can be structured to generate a small, all metal memory element, where the logical state depends on the relative orientation of the two magnetic moment directions. The magnetic element is interrogated by a 4-probe method and the resistance of the structure indicates the relative moment orientations (high resistance corresponds to antialigned moments, and low resistance corresponds to aligned moments) (17) which can be used as the memory configurations of a 2-level system. Although the illustration only depicts two magnetic layers, real magnetic devices typically are multiple repeats of this structure where the various layer orientations now represent the many memory configurations in this n-level system.

For a trilayer or multilayer structure of this type, it is clear that another area where determining magnetic structure is critical is in the determination of the order of magnetic layer switching as a function of applied filed. One technologically promising trilayer architecture, categorized as a spin valve (38), is composed of a hard magnetic layer (e.g., Co) and soft magnetic layer (e.g., NiFe alloy) separated by a nonmagnetic spacer (e.g., Cu). Since the soft magnetic layer has a lower coercive field, it should switch first leading to an antialigned state. Unfortunately, for device applications, effects such as interlayer and intralayer dipolar coupling, film micromorphology, and lithographic patterning are known to alter layer coercivities and may change the order of layer switching. Standard magnetometry techniques, which measure only the total magnetic response, can only infer the order of the layer switching indirectly. To predict device performance and understand the fundamental dynamics of the system, it is necessary to directly determine the order in which the magnetic layers switch.

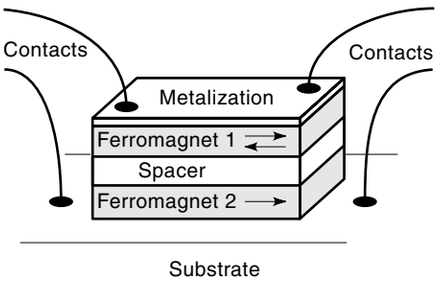

Figure 6. Prototypical magnetic-based memory element. Conductivity of all-metal device varies depending on relative orientation of two moment directions of magnetic films. Four contacts are for four-point probe interrogation.

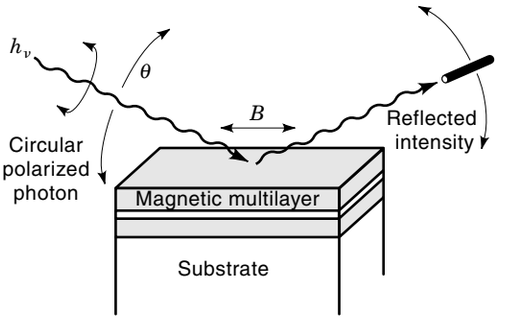

Figure 7. X-ray resonant magnetic scattering experimental geometry.

Such information is available using the technique of X-ray resonant magnetic scattering (XRMS) (39–43). XRMS is a soft X-ray reflectivity technique that involves a combination of X-ray resonant scattering and magnetic circular dichroism. In X-ray resonant scattering (XRS) (44,45), when the energy of an incident photon is equal to the binding energy of a core electron (i.e., resonantly tuned to an absorption edge), the reflectivity, or scattering factor, is greatly enhanced with respect to the nonresonant value. Using circular polarized X rays effectively combines XRS with MCD to yield a scattering technique with not only enhanced chemical selectivity but also with magnetic sensitivity and the ability to determine the magnetic depth profile of a layered system.

These reflectivity measurements were also conducted at the NRL/NSLS MCD facility located at beamline U4B of the NSLS (15). The experimental chamber consists of a vacuum compatible θ–2θ spectrometer (46) modified to incorporate a Si photo-diode detector to measure the reflected soft X-ray intensity, which is normalized to the incident photon flux as depicted in Fig. 7. Simultaneously changing the incident and detector directions allows for the acquisition of the specularly reflected intensity as a function of angle, photon energy, and applied magnetic field.

The magnetic trilayer to be studied is a NiFe(50 Å)/Cu(30 Å)/Co(20 Å) trilayer which was prepared on a Si substrate at room temperature by RF sputtering. To protect the film from oxidation, a thin Cu cap layer was deposited before the sample was removed. A standard magnetometry measurement of the NiFe/Cu/Co spin valve structure using vibrating sample magnetometry (VSM) is shown in the left panel of Fig. 8. The step in the hysteresis and the intermediate plateau regions are a clear indication of layer switching, giving rise to an antialigned state and a reduction in the total magnetization of the structure. From this measurement alone the order of the layer switching can only be indirectly inferred from knowledge of the behavior of thin films of the individual, unpatterned constituents. To directly measure the order of layer switching by XRMS, a comparison is made between the magnetic contributions to the reflectivity at the resonant energies for Co and Fe when the trilayer is in the aligned and antialigned states. The VSM data are used to determine the ap-

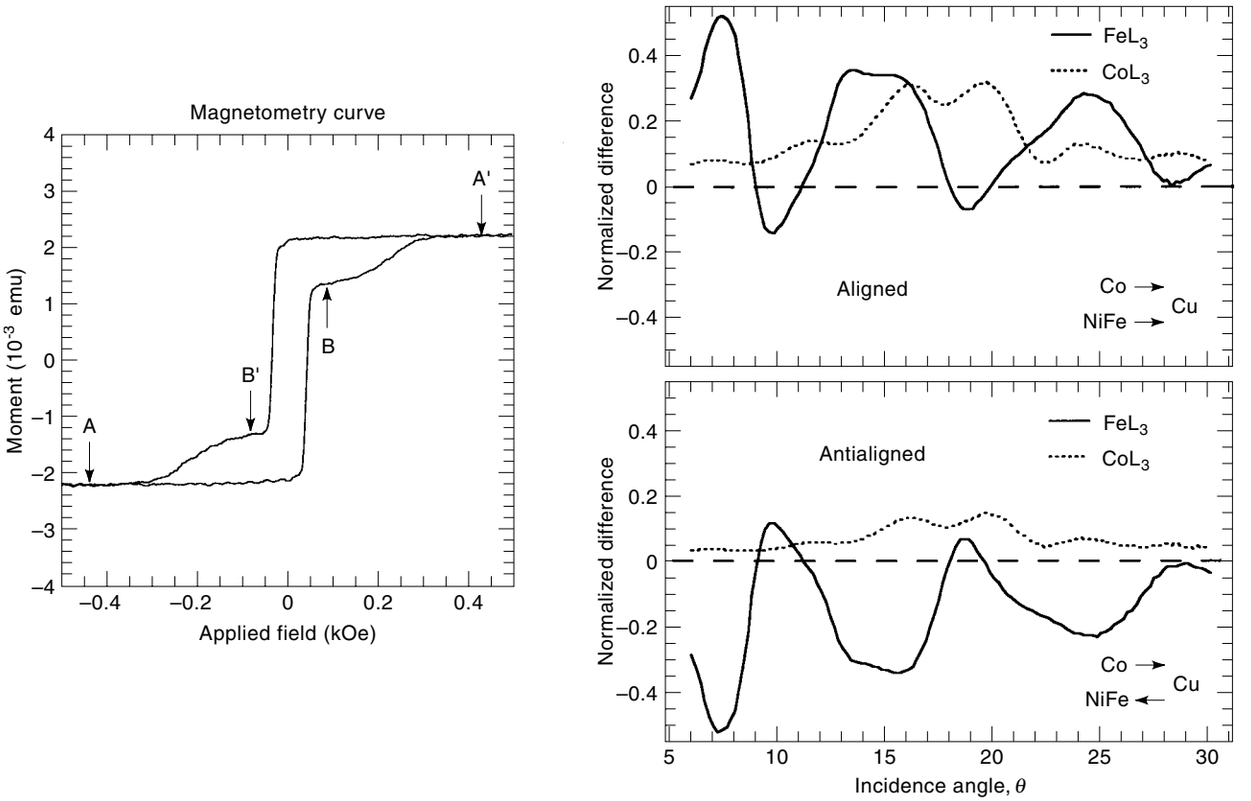

Figure 8. Determination of the order of layer switching in a Co/Cu/NiFe trilayer. Left panel shows magnetometry curve for trilayer. Top right panel shows the difference in reflectivity for Co and Fe taken at points A and A′ of the magnetometry curve. Bottom right panel shows the difference in reflectivity for Co and Fe taken at points B and B′ of the magnetometry curve and after one layer has flipped.

plied field values at which the aligned and antialigned states are realized.

For extraction of the magnetic information, it is necessary to measure the reflectivity for both left and right circular polarized light. Since there are difficulties associated with switching the helicity, it is equivalent to instead make measurements with the sample in two exactly opposite magnetic configurations while keeping the helicity fixed (9,11). For the aligned state case this is accomplished by measuring the reflectivity after applying a field large enough to saturate the sample in either magnetic field direction (marked A and A′ in Fig. 8). Reflectivity measurements of the antialigned state involves a two-step process, where it is first necessary to magnetically saturate the sample at a high field (A in Fig. 8) and then reduce and reverse the field to move along the hysteresis loop until the intermediate plateau is reached (B in Fig. 8). The measurement of the mirrored antialigned magnetic configuration is achieved by repeating the sweep in the opposite field direction (following the A′ to B′ path).

Results of the two aligned state reflectivity scans at both the Fe L_3 edge (707.5 eV) and Co L_3 edge (778.0 eV) are presented in the top right panel of Fig. 8. This panel shows the normalized difference of the measured specular reflectivity as a function of the grazing angle, θ. The magnetic information is contained in this asymmetry ratio, R, which is the normalized difference of the absorption spectra and is defined as

$$R = \frac{(I^+ - I^-)}{(I^+ + I^-)}$$

where I^+ and I^- denote the reflectivity with the magnetic structure either parallel or antiparallel to the photon helicity, respectively. The inset is a diagram of the resulting magnetization directions of the two films. The observed modulations in the difference spectra are not only due to interference effects from reflections at the various interfaces within the layered sample, they are also sensitive to the magnetic configuration of the multilayer. The lower right panel of Fig. 8 shows the normalized difference spectra for the antialigned case (B and B').

It is clearly evident that the Fe asymmetry in the antialigned case has reversed sign with respect to the aligned case, indicating that indeed the NiFe layer is the first layer to switch, as indicated by the inset. It is interesting to note, however, that even though the Co asymmetry is the same sign, it is reduced in magnitude at the lower applied field when compared to the high field value. This may indicate that the Co film is not completely antialigned to the NiFe layer but has broken into magnetic domains, in agreement with the VSM data. The lack of being in a completely antialigned state

is possibly due to dipolar magnetic coupling and/or film micromorphology.

This example has demonstrated that the order of layer switching can be determined in a multilayer system when the layers have different constituent elements. The same type of characterization can be accomplished if the ferromagnetic layers within the multilayer have the same constituent materials (47), but in this case the depth selectivity of this technique is exploited. By varying the incidence direction, the majority of the scattering occurs for the first magnetic layer at grazing incidence angles but quickly includes deeper lying layers as the angle is increased.

SUMMARY

Characterization of the magnetic structure of a system has become a critical and necessary aspect of understanding magnetic behavior of multilayer systems. As magnetic systems become increasingly complex, utilizing multiple layers with more than one magnetically active element in each, magnetic structure characterization becomes increasingly important. The utility of element-specific probes, like magnetic circular dichroism, are now clear and well demonstrated.

BIBLIOGRAPHY

1. J. B. Goodenough, *Magnetism and the Chemical Bond,* New York: Wiley, 1963.
2. R. M. Bozorth, *Ferromagnetism,* Piscataway, NJ: IEEE Press, 1978.
3. S. Chikizuma and S. H. Charap, *Physics of Magnetism,* Malabar, FL: Krieger, 1964.
4. G. A. Prinz, *Science,* **250**: 1092, 1990.
5. L. M. Falicov et al., *J. Mater. Res.,* **5**: 1299–1340, 1990.
6. H. Winick, *Synchrotron Radiation Sources: A Primer,* Singapore: World Scientific, 1994.
7. C. T. Chen, *Nucl. Instrum. Methods Phys. Res. A,* **256**: 595–604, 1987.
8. C. T. Chen and F. Sette, *Rev. Sci. Instrum.,* **60**: 1616–1621, 1989.
9. C. T. Chen et al., *Phys. Rev. B,* **42**: 7262–7265, 1990.
10. Y. U. Idzerda et al., *Phys. Rev. B,* **48**: 4144–4147, 1993.
11. Y. U. Idzerda et al., *Nucl. Instr. Methods Phys. Res. A,* **347**: 134, 1994.
12. J. G. Tobin, G. D. Waddill, and D. P. Pappas, *Phys. Rev. Lett.,* **68**: 3642–3645, 1992.
13. Y. Wu et al., *Phys. Rev. Lett.,* **69**: 2307–2310, 1992.
14. C. T. Chen, *Rev. Sci. Instrum.,* **63**: 1229–1233, 1992.
15. S. Hulbert et al., *Nucl. Instrum. Methods Phys. Res. A,* **291**: 343, 1990.
16. P. Grunberg et al., *Phys. Rev. Lett.,* **57**: 2442, 1986.
17. M. N. Baibich et al., *Phys. Rev. Lett.,* **61**: 2472, 1988.
18. C. Carbone and S. F. Alvarado, *Phys. Rev. B, Condens. Matter,* **36**: 2433, 1987.
19. J. Unguris, R. J. Celotta, and D. T. Pierce, *Phys. Rev. Lett.,* **67**: 140, 1991.
20. S. S. P. Parkin, N. More, and K. P. Roche, *Phys. Rev. Lett.,* **64**: 2304, 1990.
21. G. A. Prinz, *Ultramicroscopy,* **47**: 346–354, 1992.
22. J. Unguris, R. J. Celotta, and D. T. Pierce, *Phys. Rev. Lett.,* **69**: 1125, 1992.
23. R. A. Dragoset et al., *Mater. Res. Soc. Symp. Proc.,* **151**: 193, 1989.
24. R. H. Victora and L. M. Falicov, *Phys. Rev. B, Condens. Matter,* **31**: 7335, 1985.
25. P. M. Levy et al., *J. Appl. Phys.,* **67**: 5914, 1990.
26. D. Stoeffler, K. Ounadjela, and F. Gautier, *J. Magn. Magn. Mater.,* **93**: 386, 1991.
27. G. van der Laan and B. T. Thole, *Phys. Rev. B, Condens. Matter,* **43**: 13401, 1991.
28. K. M. Kemner et al., *J. Appl. Phys.,* **81**: 1002, 1997.
29. L. H. Tjeng et al., *J. Magn. Magn. Mater.,* **109**: 288–292, 1992.
30. C. T. Chen et al., *Phys. Rev. B, Condens. Matter,* **48**: 642, 1993.
31. Y. U. Idzerda et al., *Appl. Phys. Lett.,* **64**: 3503, 1994.
32. V. Chakarian et al., *Appl. Phys. Lett.,* **66**: 3368, 1995.
33. V. Chakarian et al., *Phys. Rev. B, Condens. Matter,* **53**: 11313, 1996.
34. M. E. Filipkowski et al., *Phys. Rev. Lett.,* **75**: 1847–1850, 1995.
35. J. C. Slonczewski, *J. Magn. Magn. Mater.,* **150** (1): 13–14, 1995.
36. J. W. Freeland et al., *Appl. Phys. Lett.,* **71**: 276, 1997.
37. J. W. Freeland et al., *J. Appl. Phys.,* **83**: 6290–6292, 1998.
38. B. Dieny et al., *Phys. Rev. B, Condens. Matter,* **43**: 1297, 1991.
39. K. Namikawa et al., *J. Phys. Soc. Jpn.,* **54**: 4099, 1985.
40. C. Kao et al., *Phys. Rev. Lett.,* **65**: 373, 1990.
41. C.-C. Kao et al., *Phys. Rev. B, Condens. Matter,* **50**: 9599, 1994.
42. J. M. Tonnerre et al., *Phys. Rev. Lett.,* **75**: 740, 1995.
43. V. Chakarian et al., *Applications of Synchrotron Radiation in Industrial, Chemical, and Materials Science,* New York: Plenum Press, 1996, p. 187.
44. D. Gibbs et al., *Phys. Rev. Lett.,* **61**: 1241, 1988.
45. E. D. Isaacs et al., *Phys. Rev. Lett.,* **62**: 1671, 1989.
46. E. D. Johnson, C.-C. Kao, and J. B. Hastings, *Rev. Sci. Instrum.,* **63**: 1443, 1992.
47. J. W. Freeland et al., *J. Vac. Sci. Technol. A, Vac. Surf. Films,* **16**: 1355–1358, 1998.

YVES U. IDZERDA
Naval Research Laboratory